Advances in Science and Technology Research Journal

Advances in Science and Technology Research Journal, 2026, 20(9), 490–506
https://doi.org/10.12913/22998624/224542
ISSN 2299-8624, License CC-BY 4.0

Received: 2026.05.17
Accepted: 2026.07.10
Published: 2026.08.01

Comparative analysis of concrete constitutive models in flexural beams using digital image correlation

Dawid Karasiewicz[1], Julia Graczyk[1], Michał Demby[1*], Szymon Wojciechowski[2]

[1] Faculty of Civil and Transport Engineering, Poznan University of Technology, 61-131 Poznan, Poland
[2] Research and Development Department, Pekabex BET S.A., 60-462 Poznan, Poland
* Corresponding author's e-mail: michal.demby@put.poznan.pl

ABSTRACT

This study investigates the influence of constitutive model parameters on both the global and local response of reinforced concrete beams. Advanced numerical simulations require appropriate material models to represent the specimen behaviour, so this research compares simplified engineering procedures with the concrete damage plasticity (CDP) model. A single representative specimen was analysed using a high-resolution digital image correlation (DIC) system to provide dense experimental data for precise calibration. The investigation focuses on identifying the specific tension stiffening description that best reflects the fracture kinematics recorded by the optical system. Results indicate that the strain-dependent approach (specifically the Massicotte model) offers superior consistency with experimental crack patterns and load-deflection curves. In contrast, models based on fracture energy exhibited unphysical blurring of damage zones and poorer crack localization. The study concludes that broad validation extending beyond global load-deflection curves, utilizing local displacement fields from DIC, is essential for an objective assessment of numerical model quality and the optimization of concrete structure design.

Keywords: concrete, concrete damage plasticity, digital image correlation, finite element method, tension stiffening.

INTRODUCTION

Concrete is a heterogeneous composite material whose nonlinear mechanical response is governed by a complex internal structure, stiffness degradation, and multi-scale fracture mechanisms. A fundamental issue in the analysis of concrete structures is the pronounced difference between high compressive strength and low tensile strength. In flexural members, critical tensile stresses are reached at relatively low load levels, leading to crack initiation and propagation deep into the cross-section, which significantly affects internal force redistribution [1,2].

Contemporary engineering practice commonly relies on simplified code procedures, such as those provided in Eurocode 2 [3]. These methods usually employ cross-sectional models in which cracking is considered through averaged reductions in bending stiffness. Although such procedures are generally safe for standard design, they are insufficient for analysing local strain concentrations, fracture kinematics, and stress redistribution in the tensile zone. For this reason, more detailed numerical approaches based on the finite element method (FEM) are required when higher accuracy or local damage assessment is needed [4,5].

A key aspect of advanced numerical simulations is the selection of an appropriate constitutive model. Among available approaches, the Drucker-Prager model has been used for concrete owing to its ability to account for the influence of hydrostatic pressure on yielding [6,7]. However, the concrete damage plasticity (CDP) model has become one of the most widely used formulations in advanced analyses of reinforced concrete. Originally proposed by Lubliner and further developed by Lee and Fenves, the model combines plasticity theory with damage mechanics and enables separate definitions of degradation processes in compression and tension [8,9]. Within the CDP framework, particular importance is assigned to the description of post-cracking tensile behaviour, commonly referred to as tension stiffening. This phenomenon results from the ability of concrete between cracks to transfer part of the tensile stresses through bond interaction with reinforcement. In numerical modelling, it may be defined using stress-strain relationships, crack-opening laws, or fracture-energy-based formulations [10,11]. The adopted softening description strongly affects numerical stability, post-cracking stiffness, crack localisation, and load-bearing capacity [12,13].

The present study analyses the influence of concrete constitutive model parameters on the global and local response of a reinforced concrete beam. Owing to the destructive character of the experimental programme, the investigation was focused on a single representative specimen. This enabled the use of a high-resolution digital image correlation (DIC) system, which provided dense full-field displacement and strain data for validation of the numerical models [14,15]. As a non-contact optical technique, DIC allows the assessment of local deformation fields with a level of detail that is not available from traditional point sensors [16,17].

Recent studies confirm the growing importance of combining experimental measurements, image-based diagnostics, and CDP simulations in the analysis of reinforced concrete elements. Krishna et al. used a CDP-based FEM model to predict the flexural response of RC beams and verified the results using load-deflection curves and DIC-based moment-curvature relationships [18]. Leppänen et al. integrated high-speed DIC measurements with damage-plasticity simulations to analyse the impact behaviour of RC beams [19]. Marzec and Bobiński compared several isotropic constitutive models and concluded that the CDP approach offered good consistency with experimental crack patterns and force-displacement curves [20]. Al-Ateyat et al. also demonstrated the usefulness of ABAQUS-based CDP simulations for reproducing the response and failure mechanisms of GFRP-reinforced concrete slabs [21], while Dejene et al. confirmed the applicability of CDP modelling to the nonlinear shear behaviour of shallow-wide concrete beams [22]. In parallel, Chu et al. highlighted the increasing role of image-based structural diagnostics by developing a UAV-based two-stage CNN system for crack detection and segmentation in GNSS-denied environments [23].

Numerical studies have also shown that tension stiffening parameters significantly influence nonlinear solutions. A sudden stress drop after cracking may alter load-deflection paths and affect crack distribution [24]. Although previous studies confirm the usefulness of CDP-based modelling and experimental validation, many analyses still focus mainly on global response indicators. The local kinematics of cracking and the direct comparison between numerical damage fields and full-field experimental strain maps remain less extensively resolved [25,26].

In this study, results obtained using simplified engineering models and basic elasto-plastic models are compared with a broad set of CDP variants. The main objective is to identify the tensile softening description that most accurately reproduces both the global load-deflection response and the local crack kinematics recorded by the DIC system. This approach extends the validation beyond global deflection curves and provides a more objective basis for assessing the quality of numerical models used in reinforced concrete analysis.

MATERIALS AND RESEARCH METHODOLOGY

Beam specification and design

The research process was initiated with a conceptual phase. The objective of this phase was the design of a reinforced concrete beam. The element was designed as a simply supported beam with an axial span of 4.0 m and a total length of 4.1 m. It operates in a four-point bending configuration. A load consisting of two concentrated forces of 40 kN each was assumed. This allows for the creation of a pure bending zone in the central part of the element. The static scheme and basic geometric dimensions are presented in Figure 1.

The dimensioning of the element was performed using engineering software. This utilized a reinforced concrete design module based on the principles of the ULS and the SLS according to the Eurocode 2 standard. C50/60 class concrete and B500B high-ductility reinforcing steel were adopted for the construction. The degree of cross-section capacity utilization under the assumed load was approximately 88% for bending.

A beam with a rectangular cross-section of 15 × 42 cm was manufactured. The main reinforcement was designed as a combination of two Ø14 bars running the full length and two additional Ø14 bars acting as supplementary reinforcement in the zone of maximum bending moment. Because of the relatively small width of the cross-section and the necessity to maintain appropriate spacing between the bars, the reinforcement was arranged in two rows. Continuity of the reinforcement and stability of the frame were achieved by Ø8 stirrups with a spacing of 25 cm. The element prepared in this manner was subjected to destructive testing using deformation measurement in addition to standard sensors, also the DIC system.

Engineering benchmark (N1)

The first stage of numerical analysis involved the development of an engineering model within a commercial engineering software environment. This model was a direct extension of the design assumptions and served as a benchmark for comparing standard design practice with advanced nonlinear simulations and experimental DIC measurements.

The engineering software used in this stage was intended primarily for structural dimensioning according to design regulations rather than for detailed nonlinear finite element analysis. Therefore, the model was based on a classical cross-sectional approach. The post-cracking stiffness of the beam was not obtained from local material degradation, as in advanced numerical models, but from simplified Eurocode 2 relationships interpolating the stiffness between State I (uncracked) and State II (fully cracked).

Material parameters corresponding to C50/60 concrete and B500B reinforcing steel were adopted. The response obtained from this model is global in nature: it provides the elastic-plastic deflection of the member but does not generate crack maps, local stress concentration zones, or detailed strain redistribution fields. Despite these limitations, the engineering model remains an important reference because it represents calculations routinely performed in structural design practice. Its comparison with the DIC measurements and nonlinear FEM results makes it possible to assess where the normative approach is sufficient and where more advanced constitutive modelling is required.

General assumptions of the numerical model

The primary objective of this stage was to replicate the structural behaviour of the beam as accurately as possible. The modelling process required a detailed approach to both geometric discretization and the definition of contact conditions [27, 28].

The beam was modelled as a three-dimensional object using eight-node solid elements with reduced integration. These are designated as SOLID C3D8R elements. Reinforcement within the numerical model was incorporated using the Embedded Region technique. The reinforcing bars were modelled as beam elements which were embedded within the concrete volume. This approach assumes a perfect bond between the steel and concrete. Given the standard anchorage lengths and the absence of slip phenomena in the experimental study, this simplification is considered fully justified.

The components of the experimental apparatus including the supports and the loading traverse were treated as rigid bodies. The stiffness of the steel used for the laboratory equipment is orders of magnitude higher than that of the tested beam. Therefore, neglecting its deformability does not affect the results and significantly enhances the

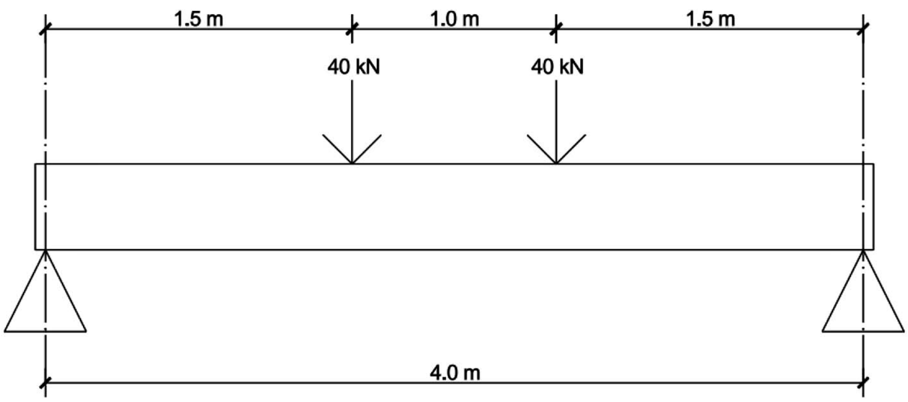

Figure 1. Static diagram and geometric dimensions of the tested beam

numerical stability of the model. The interaction between the steel plates and the concrete surface of the beam was defined as surface-to-surface contact. This accounted for the coefficient of friction, which facilitates a realistic rotation of the beam at the supports (Figure 2). The analysis was performed using a static general procedure. One of the most critical challenges involved ensuring numerical convergence during the concrete cracking phase. The minimum time increment was established at 1E-5 [-]. Displacement control of the loading traverse was utilized to apply the load to the beam. This strategy facilitated a stable transition through the concrete softening phase following the attainment of ultimate capacity. It also permitted the recording of the complete load-deflection relationship including the post-critical range. This was essential for obtaining comprehensive strain fields. These fields were subsequently superimposed onto the data maps generated by the DIC system.

Basic constitutive models

A total of seven variants of numerical models were developed. These differed in the constitutive description of concrete while maintaining constant parameters for the steel reinforcement. The reinforcement was defined based on the characteristic parameters of B500B steel. An elastic-plastic model featuring a clearly defined plastic plateau and linear hardening was adopted. Young's modulus for steel was set at E_S = 200 GPa, and the Poisson's ratio was taken as 0.3 (Figure 3).

The reliability of the model was ensured by basing the concrete parameters on actual laboratory tests rather than design assumptions alone. Static compression tests performed on specimens indicated that the actual mean compressive strength of the concrete was f_{cm} = 65.83 MPa. This indicates that the applied mixture achieved a higher strength class than the originally assumed C50/60. Based on the recorded mean strength, the remaining parameters were determined using the relationships provided in Eurocode 2. These include a Young's modulus of E_c = 38.72 GPa, a tensile strength of f_{tm} = 4.29 MPa, and specific ultimate strain values. The Poisson's ratio for concrete was adopted as 0.2.

Bi-linear model (N2)

The first and most simplified approach involved a perfectly elastic-plastic model. This is hereinafter referred to as the bilinear model (N2). This model is based directly on the simplified normative assumptions contained in Eurocode 2.

In this model, concrete is treated as an isotropic material with linear-elastic characteristics until the mean compressive strength is reached. Upon exceeding this value, the material enters a phase of pure plastic flow. Consequently, stresses in the concrete remain at a constant level. This is the so-called plastic plateau. In this state, strains increase until ultimate limit values are reached, after which immediate failure of the element occurs (Figure 4). Because of its simplicity, the bilinear model (N2) does not account for the phenomenon of material softening or stiffness degradation. Both are key characteristics of actual concrete behaviour. Furthermore, it omits a complex description of concrete behaviour in tension. This omission typically leads to an overestimation of the stiffness of the member during the cracking phase.

Drucker-Prager model (N3)

The subsequent stage of the analysis involved the application of the Drucker-Prager model (N3). This model represents a more advanced approach than the bilinear method because it introduces the dependency of the yield surface on hydrostatic pressure. It has achieved extensive recognition in

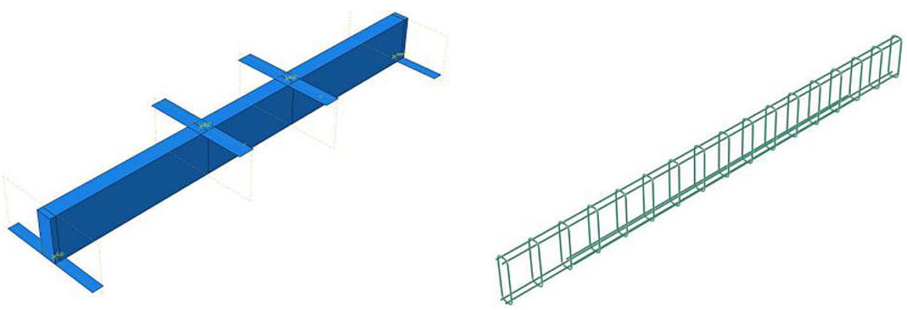

Figure 2. Discrete model of the beam and reinforcement in the engineering program

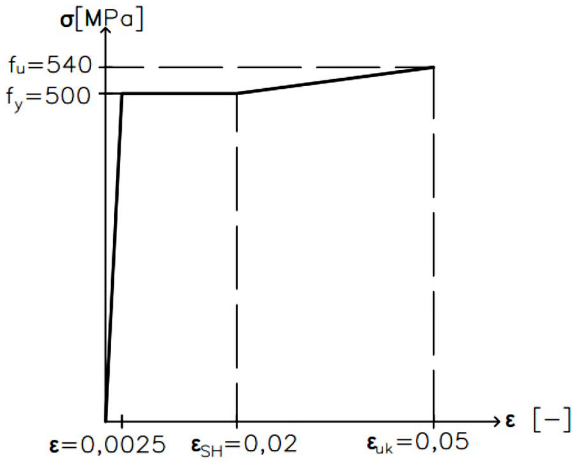

Figure 3. The assumed stress-strain diagram for reinforcing steel

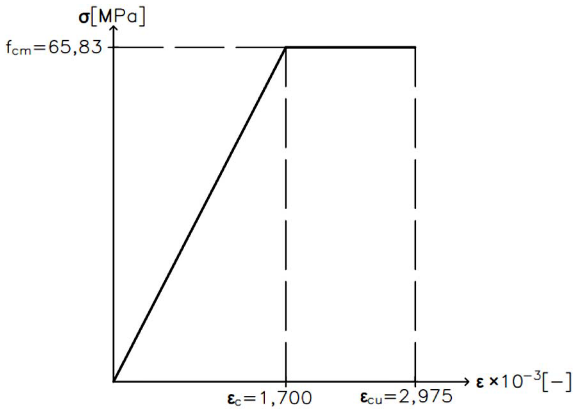

Figure 4. Adopted stress-strain relationship of concrete for the bilinear model (N2)

the modelling of brittle and semi-brittle materials. In contrast to the bilinear model (N2), which assumes a constant stress level upon reaching the yield point, the Drucker-Prager model (N3) incorporates a more realistic and nonlinear characteristic for concrete. In accordance with Eurocode 2 guidelines, concrete behaviour in the initial phase was assumed to be linear-elastic up to a level of 0.4 f_{cm}. Beyond this threshold, a curve defined by the following equation was implemented in the model:

$$\frac{\sigma_c}{f_{cm}} = \frac{k\eta-\eta^2}{1+(k-2)\eta} \tag{1}$$

where:

$$\eta = \frac{\varepsilon_c}{\varepsilon_{c1}} \tag{2}$$

$$k = 1.05E_{cm}\frac{\varepsilon_{c1}}{f_{cm}} \tag{3}$$

The application of this function enabled the representation of the hardening phase and the initial softening phase of the material. This representation is critical for the accurate determination of beam stiffness under high stress states (Figure 5).

The implementation of the Drucker-Prager model (N3) within the FEM software necessitates the definition of specific material parameters. Based on a review of the relevant literature, the following values were adopted for the model [29, 30]:

- Internal friction angle φ = 38° – this parameter defines the inclination of the yield surface in the principal stress space
- Flow stress ratio K = 0.78 – a parameter defining the shape of the yield surface on the deviatoric plane.
- Dilation angle α = 12° – a parameter specifying the volumetric increase of the material during plastic flow.

Development of CDP (N4-N8)

The most advanced and pivotal numerical tool utilized in this research was the CDP model. The

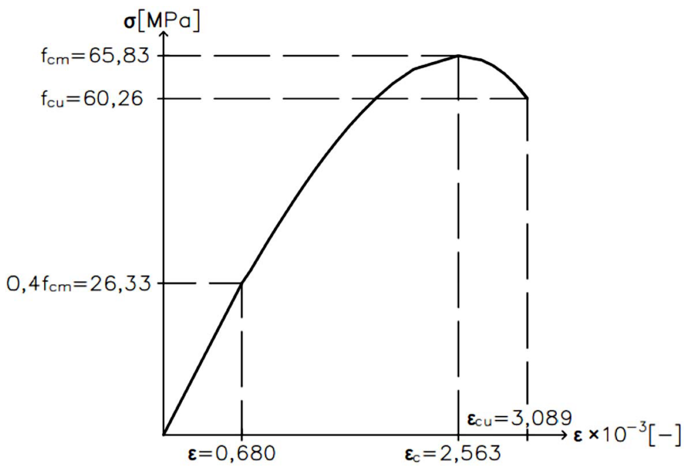

Figure 5. Adopted nonlinear concrete characteristic for the Drucker-Prager model

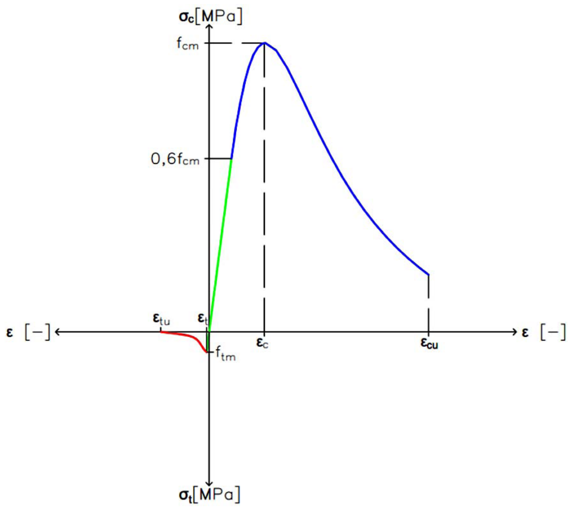

Figure 6. Constitutive behaviour of concrete in the CDP model

selection of this model was dictated by its unique ability to simultaneously describe the two dominant failure mechanisms of concrete which are plastic flow and cracking. Consequently, the CDP model enables the analysis of nonlinear stress-strain relationships and the reproduction of material stiffness degradation. It also allows for the crack-closure effect under load reversal [31, 32].

In the CDP model, concrete behaviour is described within three fundamental ranges:

- Linear-elastic range: This corresponds to the initial loading stage where the material maintains a constant stiffness defined by the initial Young's modulus. At this stage, strains are fully reversible and no material damage occurs.
- Nonlinear range in compression: This describes the plastic hardening phase of concrete from the initiation of microcracks until the compressive strength is reached. In this study, an identical compression curve was adopted across all five numerical variants to maintain comparative clarity. This allowed for the isolation of the influence of the tension description on the global beam response.
- Softening range: This is the stage after the tensile strength threshold is exceeded. It is characterized by a gradual degradation of the capacity of the material point. Various descriptive strategies were implemented specifically within this range (Figure 6).

The compressive characteristic of concrete was defined using a nonlinear formula proposed by Sargin [33]. To regulate material softening, a damage parameter D with a value of 0.75 was applied. The expression for the curve is as follows:

$$\sigma_c = \frac{\frac{E_{cm}}{E_g}\cdot\frac{\varepsilon}{\varepsilon_c}+(D-1)\cdot\left(\frac{\varepsilon}{\varepsilon_c}\right)^2}{1+\left(\frac{E_{cm}}{E_g}-2\right)\cdot\frac{\varepsilon}{\varepsilon_c}+D\cdot\left(\frac{\varepsilon}{\varepsilon_c}\right)^2}\cdot f_{cm} \tag{4}$$

where:

$$E_g = \frac{f_{cm}}{\varepsilon_c} \tag{5}$$

In addition to the definition of the material curves, the CDP model requires the specification of five key parameters controlling the shape of the yield surface and the flow potential (Figure 7). Based on an extensive literature review and results from studies with similar research themes, the following values were adopted [34,35]:

- dilation angle α = 12: This parameter determines the volumetric increase of concrete subjected to plastic compression. The selected value is typical for high-strength concretes;
- eccentricity ε = 0.1: A parameter defining the rate at which the plastic potential surface approaches the asymptote;

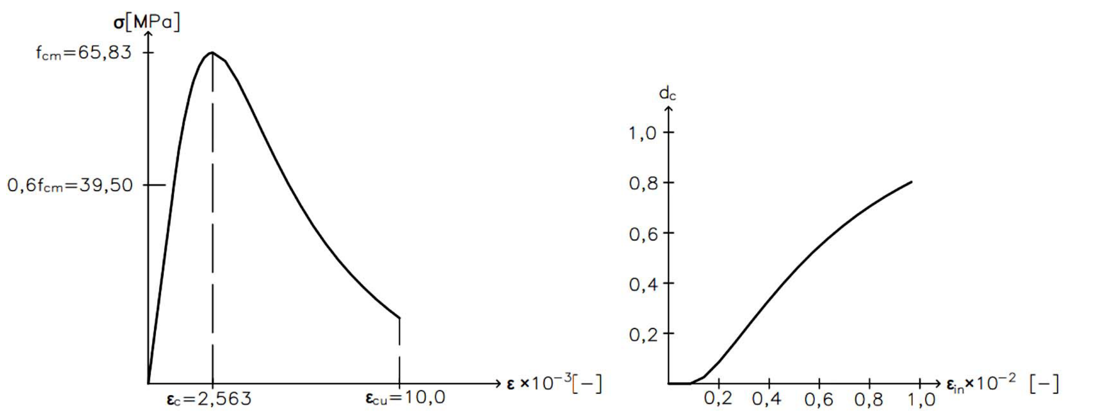

Figure 7. Stress-strain relationship and damage parameter evolution in the CDP model under compression

- biaxial to uniaxial strength ratio $f_{b,0}/f_{c,0}$ = 1.16: A standard value for concrete that defines the initial yielding point under biaxial compression;
- parameter K = 0.6667: Defines the shape of the yield surface on the deviatoric plane. This value ensures that the yield surface remains convex.
- viscosity parameter μ = 0.0001: Utilized for the regularization of equations during the softening phase. This low value maintains computational convergence during rapid crack propagation without excessively distorting the static results.

In the analysed reinforced concrete beam, the method of describing tension is of decisive importance for the moment of cracking and the final deflection. It also affects the precision of the strain fields recorded by the DIC system. While the compression parameters remained constant, several variants of the tension definition were analysed in detail in the subsequent sections. This facilitated a unique verification of whether an approach based on fracture energy or direct modelling through crack opening yields results closer to the actual strain maps obtained from the optical measurement system.

Massicotte model (N4)

The first analysed variant for describing concrete behaviour in tension, implemented within the CDP model framework, was a bilinear function defined in the strain domain. This approach is based on the proposal formulated by B. Massicotte and co-workers. It was developed for simplified yet effective tension modelling [36, 37].

This model is particularly valued in numerical engineering analyses because of its relative simplicity of implementation and the minimal number of required input parameters. The definition of the curve is based on the elastic limit strain ε_{cr}, which corresponds to the moment the tensile strength f_t is reached. Based on this value and by utilizing empirical relationships proposed by the authors, the complete softening function is constructed. It consists of two linear segments with different slopes (Figure 8). As part of the numerical implementation in the engineering software, it was also necessary to define the tensile damage parameter d_t. This parameter was determined approximately based on the relationship between post-cracking stresses and the initial material stiffness [38].

It should be noted that although the final stress in the element reaches zero and the damage parameter should theoretically equal 1.0, achieving this exact value is not possible in practice. This is due to purely numerical reasons. Reaching d_t = 1.0 would signify a complete loss of material stiffness. In the finite element method, this would lead to issues such as stiffness matrix singularity or numerical instability. In practice, values very close to unity like 0.99 are adopted.

Linear crack-opening function (N5)

Another variant analysed for describing the tensile zone of concrete is a linear model defined in the crack-opening domain w. This approach is based on the concept of a fictitious crack, which is fundamental to fracture mechanics.

In contrast to classical stress-strain relationships, once the tensile strength is exceeded, the material relation is defined as a function of the tensile stress versus the crack opening width. In the linear model, it is assumed that after crack initiation the stresses transmitted across the crack faces decrease linearly with increasing opening. This continues until the complete loss of material cohesion (Figure 9) [39].

The key parameter in this approach is the fracture energy G_f, which geometrically corresponds to the area under the σ – w curve.

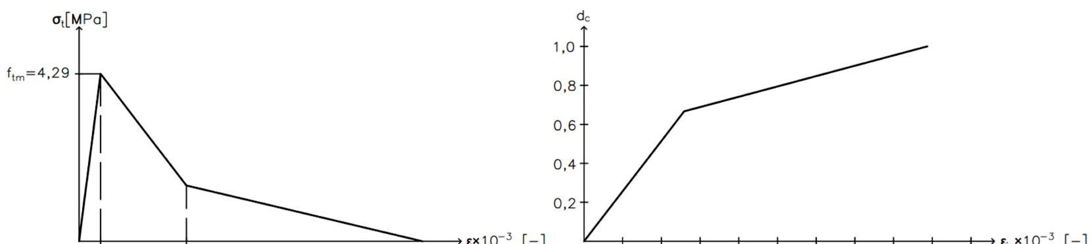

Figure 8. Concrete tensile characteristics in the CDP model according to Massicotte: (a) $\sigma - \varepsilon_{cr}$, relationship, (b) evolution of the damage parameter d_t

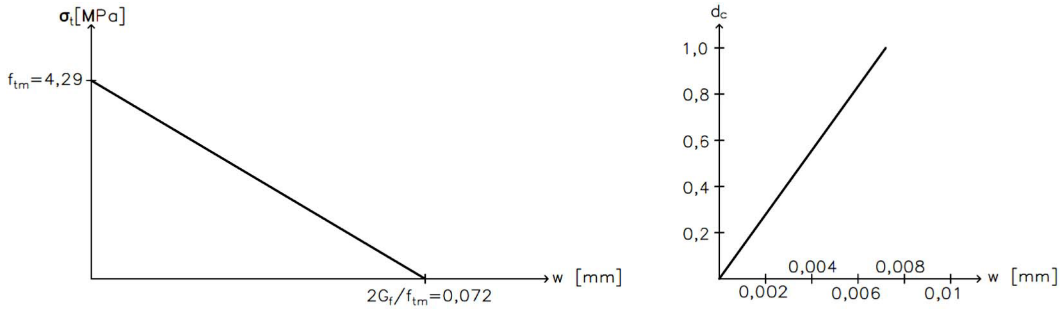

Figure 9. Tensile behaviour as a function of crack opening: (a) linear softening curve σ – w, (b) evolution of the damage parameter d_t

Physically, G_f is defined as the amount of energy required to create a unit area of crack through the complete separation of the material faces. This parameter is extremely important because it reflects the ductility of concrete in the cracked phase. A higher value of G_f results in a slower degradation of the load-carrying capacity of the element. Accurate determination of the fracture energy requires specialist laboratory testing. Therefore, empirical relationships are commonly used in engineering practice.

The value of G_f depends on many factors, where the most important are the concrete strength class and the maximum aggregate size. For ordinary concretes of average strength, the value of G_f typically lies in the range 50–200 N/m [40]. In the present analysis, the fracture energy was determined from the empirical relationship recommended by the Model Code [41]. This was based on the parameters of the concrete mix used during the fabrication works.

$$G_F = 73 \cdot f_{cm}^{0,18} = 155.11\ \mathrm{N/m} \tag{6}$$

Implementation of this model required defining the damage parameter d_t as a function of the crack opening. As in the preceding variants, a simplified approach was applied. It was based on the ratio of the stress to the tensile strength.

Bilinear crack-opening function Hillerborg model (N6)

Another variant of the concrete softening description implemented in the CDP model was a bilinear function defined in the crack-opening domain. This follows the concept of Hillerborg [42]. In contrast to the simple linear model, the σ – w relationship here consists of two straight-line segments with different slopes (Figure 10). The value of the total fracture energy G_f was adopted at the same level as in the linear model. This enabled a direct comparison of the influence of the softening function shape alone on the beam behaviour.

Exponential crack-opening function Cornelissen model (N7)

The most advanced variant used in the analysis for describing the tensile zone was the exponential function proposed by Cornelissen et al. [43]. This model is widely regarded as one of the most accurate representations of actual concrete behaviour. It smoothly captures the progressive and nonlinear degradation of material load-carrying capacity after cracking. It was developed based on extensive experimental investigations of concrete (Figure 11). The constitutive relationship

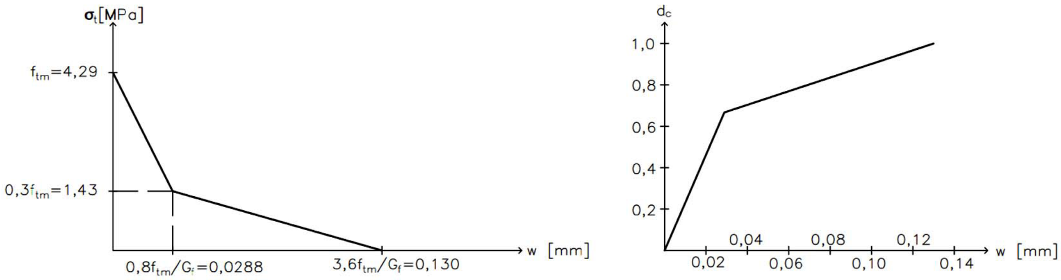

Figure 10. Tensile behaviour according to Hillerborg: a) bilinear softening curve σ – w, b) evolution of the damage parameter d_t

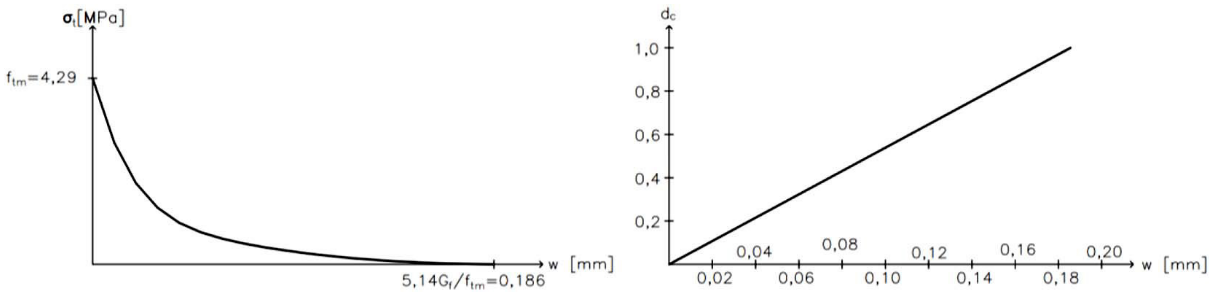

Figure 11. Tensile behaviour according to Cornelissen: a) exponential σ – w curve, b) evolution of the damage parameter d_t

in this model takes the form described by the following equation:

$$\frac{\sigma}{f_t} = f(w) - \frac{w}{w_c} f(w_c) \tag{7}$$

$$f_{(w)} = \left[1 + \left(\frac{c_1 w}{w_c}\right)^3\right] \exp(-\frac{c_2 w}{w_c}) \tag{8}$$

where: w – crack opening [m], w_c – critical crack opening [m], c_1 – material constant c_1 = 3.0 for ordinary concrete, c_2 – material constant c_2 = 6.93 for ordinary concrete.

During the implementation of the Cornelissen model in the FEM environment, significant numerical difficulties were encountered in defining the tensile damage parameter d_t. Several nonlinear damage evolution curves were tested by modifying the number and position of the defining points, including highly simplified two-point approximations. However, these attempts led to convergence problems and non-physical negative plastic strains. Therefore, to ensure numerical stability during intense cracking, a linear evolution function for d_t was finally adopted, while the exponential stress-crack opening law of the Cornelissen model was retained.

Model based directly on fracture energy (N8)

The last of the adopted nonlinear modelling strategies was a variant based on the direct definition of the fracture energy G_f as the key constitutive parameter. In contrast to the previous approaches where concrete softening was described by means of explicit functions, the program here automatically regulates the load-carrying capacity degradation process. This is based on the energy potential required for the complete opening of a crack within a given finite element.

To maintain strict physical consistency with the earlier models that employed the crack-opening concept, a constant value of the fracture energy was adopted in all analyses. In this way, the stiffness degradation process in the post-critical phase is described by the same energy potential regardless of the specific formulation.

TEST SETUP AND EXPERIMENTAL PROCEDURE

The beam was tested in a four-point bending configuration using a laboratory setup that enabled controlled load application and simultaneous recording of force, displacement, and

Figure 12. Experimental setup

full-field deformation data. A schematic of the test setup is shown in Figure 12. The specimen was simply supported on two steel supports with elastomeric bearing pads, while the load was applied through a spreader beam.

The mid-span deflection of the beam was measured using a displacement transducer (LVDT) positioned against the bottom edge of the specimen (L1). In parallel, the actuator force was recorded. Full-field deformation measurements were carried out using a Digital Image Correlation system (L2). Before testing, the lateral surface of the beam was painted white and covered with a black stochastic speckle pattern.

The DIC measurements were performed using an ARAMIS 12M (USB) optical system in a 2D measurement configuration. The analysed measurement field corresponded to the lateral surface of the beam and was processed using a manually defined scale of 1.303 mm/pixel. The analysed image area had a resolution of 4096 × 1000 px, and 10531 images were recorded during the deformation measurement. The resulting full-field displacement and strain maps were used for comparison with the numerical results.

To ensure a consistent comparison between the experimental DIC data and the CDP simulations, the FEM model reproduced the beam geometry, reinforcement layout, boundary conditions, and four-point bending scheme used in the laboratory test. The strain-field comparison was performed at the same load level of 80 kN, corresponding to the design load selected for crack-pattern evaluation. The numerical damage fields were extracted from the same lateral surface of the beam monitored by the DIC system, which allowed the experimental strain maps to be directly compared with the corresponding tensile damage or equivalent plastic strain distributions obtained from the FEM model.

RESULTS

Mesh sensitivity study

In nonlinear numerical analyses of concrete structures, the selection of an optimal finite element size is of fundamental importance. This issue extends beyond the mere accuracy of geometric approximation. For brittle and quasi-brittle materials exhibiting softening behaviour, the mesh size directly influences the objectivity of the obtained solution. Without a proper convergence study, the simulation results may become dependent on the adopted discretisation instead of reflecting the actual structural response [44, 45].

The CDP model with the Massicotte softening function (N4) was deliberately selected for the sensitivity analysis. This choice was dictated by the fact that the Massicotte model (N4) is defined directly in the strain domain. This differs from the fracture-energy-based variants described earlier. In this formulation, the fracture energy contained within a single finite element is the product of the area under the constitutive curve and the characteristic element length L_e. This renders the model particularly susceptible to discretisation-induced errors [46].

Four discretisation variants were prepared for the study. These are designated as Mesh 1 (M1) through Mesh 4 (M4). They differed in the refinement level applied to both the concrete beam and the reinforcing bar discretisation. The detailed geometric parameters of the finite elements are summarised in Table 1.

The primary criterion for assessing convergence was the global structural response expressed by the load-deflection relationship at the beam mid-span. Figure 13 presents the curves obtained for all four variants.

Analysis of the plots permits several important observations. In the initial loading phase,

Table 1. Finite element sizes adopted in the mesh sensitivity analysis

Mesh variant	Longitudinal element size	Transverse (width) element size [mm]	Height-direction element size [mm]	Reinforcement element size [mm]
Mesh 1 (M1)	$\frac{L}{50}$ (82 mm)	$\frac{b}{2}$ (75 mm)	$\frac{h}{6}$ (70 mm)	$\frac{L}{50}$ (82 mm)
Mesh 2 (M2)	$\frac{L}{64}$ (64 mm)	$\frac{b}{3}$ (50 mm)	$\frac{h}{7}$ (60 mm)	$\frac{L}{64}$ (64 mm)
Mesh 3 (M3)	$\frac{L}{100}$ (41 mm)	$\frac{b}{4}$ (37,5 mm)	$\frac{h}{10}$ (42 mm)	$\frac{L}{100}$ (41 mm)
Mesh 4 (M4)	$\frac{L}{128}$ (32 mm)	$\frac{b}{5}$ (30 mm)	$\frac{h}{14}$ (30 mm)	$\frac{L}{128}$ (32 mm)

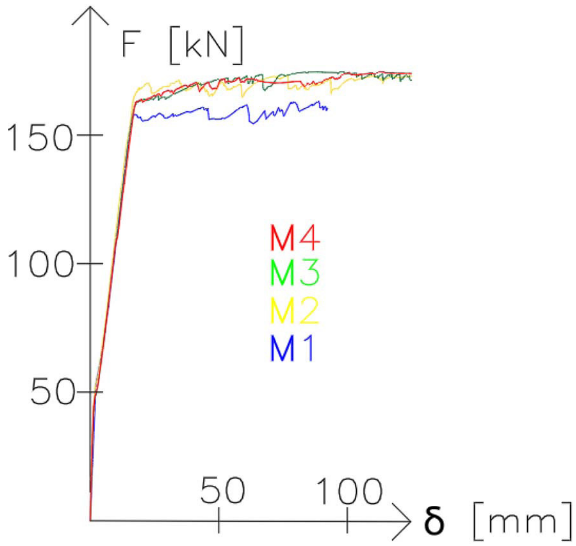

Figure 13. Comparison of load-deflection relationships for various finite element mesh densities

all four models exhibit nearly identical stiffness. The crucial differences emerge at the moment of first crack initiation. The coarsest mesh variant (M1) is characterised by a premature loss of load-carrying capacity. This stems from the fact that excessively large finite elements are incapable of correctly capturing the steep strain gradient in the tensile zone. This leads to an artificial averaging of damage over an overly large volume.

With progressive mesh refinement in variants M2 and M3, the numerical response undergoes stabilisation. The most important finding is the close convergence of results between variants M3 and M4. Based on the conducted analyses, Mesh 3 (M3) was adopted for all subsequent comparative calculations. This decision is justified on both technical and economic grounds. The selection of mesh M3 represents an optimal compromise between numerical accuracy and computational cost. It enables reliable validation of the advanced concrete constitutive models in the subsequent stages of the work.

Comparison of load-deflection response

The primary criterion for assessing the effectiveness of the implemented modelling strategies was a detailed examination of the beam deflection. This is treated as the fundamental indicator of the global structural response. Figure 14 presents the complete set of load-deflection curves obtained experimentally and numerically for all eight modelling variants. The reference value for the relative error calculations was taken from the displacement transducer (LVDT) mounted at the beam mid-span. This sensor recorded a deflection of exactly 8.84 mm at the control load of 80 kN, which is the design load for which the beam was originally dimensioned. This measurement was considered the most reliable owing to the direct nature of data acquisition and the physical contact between the sensor and the bottom concrete surface. Importantly, the results obtained in parallel by Digital Image Correlation showed very high agreement with the LVDT reading. The DIC system yielded a value of 9.01 mm, which corresponds to a relative difference of 1.96%. The virtually identical course of the two experimental curves over the full loading

Table 2. Summary of deflection values at an 80 kN load

Analysis variant	Deflection [mm]	Relative difference [%]
Experimental measurements		
LVDT (L1)	8.84	-ref.
DIC (L2)	9.01	+1.96
Engineering and simplified models		
Engineering model - EC2 (N1)	11.94	+35.10
Bilinear plasticity (N2)	2.00	−77.34
Drucker-Prager (N3)	2.00	−77.34
CDP models		
CDP - Massicotte (N4)	7.39	−16.40
CDP - Linear softening (N5)	5.32	−39.83
CDP - Hillerborg (N6)	5.96	−32.53
CDP - Cornelissen (N7)	6.70	−24.22
CDP - Fracture energy G_f (N8)	5.22	−40.95

range confirms the high quality of the reference data and the repeatability of the measurement techniques. Table 2 provides a summary of the deflection values at 80 kN. This serves as the basis for the interpretation of the constitutive model behaviour.

A detailed analysis of the CDP model results (N4-N8) revealed significant differences in the ability of formulations to represent the nonlinear behaviour of concrete. The highest agreement with the experimental data was achieved by the Massicotte model (N4). This variant recorded a deflection of 7.39 mm, which is a deviation of 16.40%. This variant most accurately reproduced the initial stiffness and the characteristics of the nonlinear phase. This includes post-cracking stiffness degradation. The Cornelissen model (N7) yielded a deflection of 6.70 mm, which corresponds to an underestimation of 24.22%. It should be noted that in this case the analysis terminated prematurely because of a loss of numerical stability. This was caused by reaching the minimum specified time increment.

The Hillerborg model (N6) exhibited superior numerical stability in the post-cracking range. However, it provided a lower accuracy in deflection estimation at 5.96 mm, which is an error of 32.53%. Its response exhibited an overly smooth load-deflection curve that lacked the irregularities observed experimentally. The largest underestimations among the CDP variants were recorded for the linear softening (N5) and the direct fracture energy (N8) approaches. These yielded deflections of 5.32 mm and 5.22 mm. Although the linear softening function offered

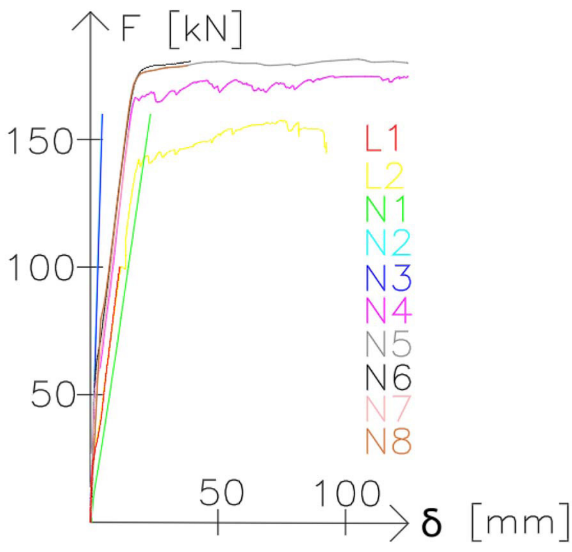

Figure 14. Load-deflection curves for all analysed models

the highest computational efficiency, both formulations proved excessively stiff in the nonlinear range. They failed to adequately capture the progressive stiffness degradation caused by cracking.

The study also included a simplified cross-sectional engineering model (N1) based on the procedures of Eurocode 2. The resulting deflection of 11.94 mm represents an overestimation of 35.10%. Despite this deviation, the result lies on the safe side from a design perspective. This confirms the conservative character of standard code-based methods. At the opposite extreme were the models based on classical plasticity theory (N2) and the Drucker-Prager criterion (N3). These models drastically underestimated the deflection to approximately 2.0 mm, which is an error of 77.34%. These findings confirm the inadequacy of classical plasticity models that lack a damage parameter for the analysis of reinforced concrete flexural members. Without accounting for elastic stiffness degradation, the simulation is unable to represent the actual material behaviour. This renders such models unsuitable for analysing the inelastic response of beams in bending.

Comparison of cracking patterns

A further key stage in the verification of the adopted modelling strategies was a detailed analysis of the morphology and character of the beam cracking. Whereas the comparison of deflections enabled an assessment of the global stiffness, it was only the analysis of the local damage fields that made it possible to check whether the numerical models correctly reproduce the physics of concrete fracture. The comparison of all variants with the experimental results was carried out for a load of 80 kN. This corresponds to the load level for which the member was originally dimensioned.

It is worth noting at the outset that no plastic response of the material was recorded for the load level considered in the case of the simplest numerical models (N2-N3). The lack of a measurable numerical response precluded the generation of crack maps. This resulted in these variants being excluded from the subsequent comparative analysis. In the remaining CDP models (N4-N7), the tensile damage index (DamageT) was adopted as the primary parameter describing the evolution of damage. This parameter enables visualisation of the zones in which degradation of material stiffness has occurred. The exception was the model based directly on fracture energy

Table 3. Semi-quantitative comparison of crack-pattern characteristics at 80 kN

Model	Number of dominant cracks [-]	Mean crack spacing [mm]	Length of cracked zone [mm]	Maximum vertical extent of cracking [mm]
CDP - Massicotte (N4)	19	148	2665	336
CDP - Linear softening (N5)	15	148	2069	255
CDP - Hillerborg (N6)	15	159	2227	294
CDP - Cornelissen (N7)	17	138	2212	284
CDP - Fracture energy G_f (N8)	11	207	2071	292
DIC (L2)	20	119	2260	323

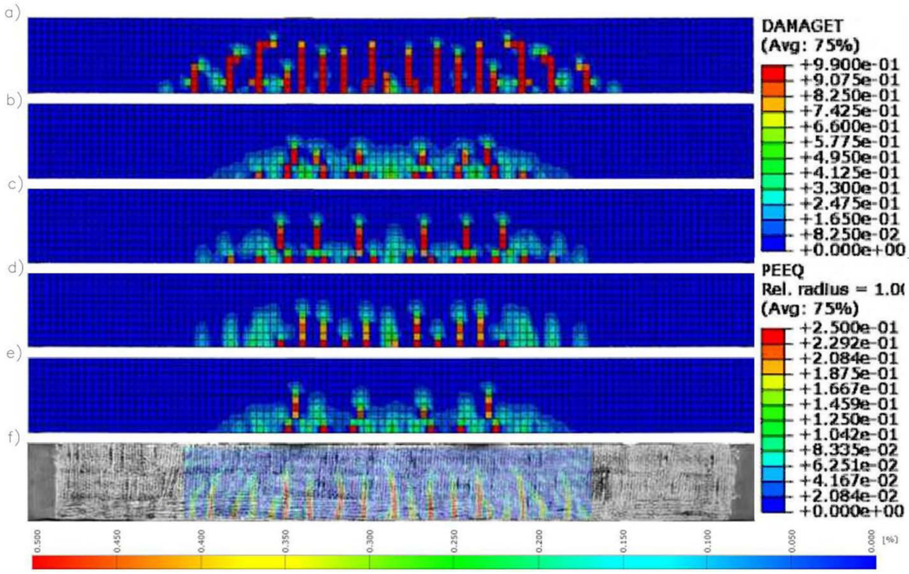

Figure 15. Comparison of numerical failure indicators and experimental DIC strain field: (a–d) tensile damage parameter (DamageT) for CDP models N4–N7, respectively; (e) equivalent plastic strain (PEEQ) for model N8; (f) DIC strain map

(N8). Owing to the absence of a defined stiffness degradation function, the equivalent plastic strain (PEEQ) was adopted as the measure of damage in this variant (Figure 15, Table 3).

The semi-quantitative comparison confirms that the Massicotte model (N4) provided the closest overall agreement with the DIC results. This model reproduced a similar number of dominant cracks to the experimental strain map, with 19 cracks compared with 20 cracks identified in the DIC field. It also provided the closest estimate of the maximum vertical extent of cracking, equal to 336 mm compared with 323 mm in the experiment. Although the longitudinal extent of the cracked zone was overestimated by the Massicotte model, the damage morphology remained clearly localised and allowed individual flexural cracks to be distinguished. In contrast, the variants based on crack-opening and fracture-energy formulations generated more diffuse damage patterns. In the linear softening (N5), Hillerborg (N6), and Cornelissen (N7) models, the damage zone typically covered a broader band of finite elements, which visually manifested itself as crack blurring. Among these models, the Hillerborg (N6) and Cornelissen (N7) variants provided a cracked-zone length closer to the DIC result than the Massicotte model. However, they underestimated the number of dominant cracks and produced less distinct crack separation. This reduced their ability to reproduce the dense and clearly localised crack network observed experimentally.

The least favourable agreement with the DIC data was obtained for the model based directly on fracture energy (N8). The cracking zone, represented by the equivalent plastic strain field (PEEQ), was less developed and concentrated in fewer locations than in the experimental strain map. This variant produced only 11 dominant cracks and the largest mean crack spacing, equal to 207 mm. Therefore, it did not reproduce the dense crack network recorded by the DIC system. The observed tendency of the energy-based models to produce more diffuse damage zones can be explained by the fracture energy regularisation concept. In these formulations, the energy dissipated during cracking is distributed over the characteristic length of the finite element. This stabilises the global post-cracking response and limits mesh-dependent energy dissipation, but it may also spread damage over a finite band of elements rather than forming sharply localised cracks. Therefore, energy-based models may provide stable global responses while being less precise in reproducing individual crack paths observed in DIC maps. Overall, the comparison confirms that CDP models employing explicit softening functions offer considerably greater informational value for diagnostic and validation purposes than simplified plasticity-based models. The Massicotte model (N4) provided the best overall representation of the experimentally observed crack density, localisation character, and vertical development of cracking.

Beam load-carrying capacity

All the numerical models analysed exhibit a tendency to somewhat overestimate the ultimate load-carrying capacity of the beam. Since the failure mechanism observed in the laboratory was crushing of concrete in the compression zone, the global response of the model in the limit state was governed decisively by the adopted concrete compressive characteristics instead of the tensile parameters. Despite the use of the actual mean concrete strength obtained from material tests, the numerical capacity still exceeds the experimental values. This discrepancy likely arises from inherent numerical model idealizations, which assume a perfect reinforcement bond and flawless cross-sectional geometry. The simulation neglects minor fabrication errors, such as formwork dimensional inaccuracies, the non-ideal assembly and alignment of the reinforcement cage, and its micro-displacements occurring during concrete casting and vibration

The comparative study demonstrated that the predictive capability of numerical models for reinforced concrete beams in flexure is strongly governed by the description of concrete behaviour in tension and by the mathematical form of the tension softening function. The differences between the analysed constitutive models were not limited to global quantities such as mid-span deflection but also affected strain localisation and crack morphology. The best agreement with the experimental data was obtained using the CDP model with the strain-dependent Massicotte softening function (N4). This applies to both global stiffness and local fracture kinematics. The effectiveness of this approach can be attributed to the fact that strain-based softening promotes sharper deformation localisation within a limited number of finite elements. As a result, distinct flexural cracks were formed, which corresponded well with the narrow strain concentration bands recorded by the DIC system. However, models of this type are sensitive to the adopted finite element size because they do not include automatic fracture energy regularisation. Therefore, the dissipated energy may depend on the element volume, which makes a mesh sensitivity study necessary. In contrast, the models based on stress-crack opening relationships (N5-N7) exhibited higher numerical stability. This advantage results from the direct control of fracture energy, which improves the objectivity of global energy dissipation and supports convergence in the post-cracking range. However, this regularisation may also distribute the degradation process over the characteristic length of the finite element, leading to a wider damage band instead of sharply localised individual cracks. Consequently, these models may reproduce the global response in a stable manner, but they tend to provide a less distinct representation of crack paths when compared with DIC strain maps.

The direct fracture energy model (N8) represents a specific implementation of the energetic approach. Despite its sound theoretical basis, it showed the weakest agreement with the experimental crack pattern. This may be related to the simplified implementation and the lack of direct control over the evolution of the damage variable, which limited its ability to reproduce the progressive degradation and dense crack network observed during the laboratory test. An important finding of this study is the inadequacy of classical plasticity models (N2-N3) for the analysis of cracked reinforced concrete members. The absence of a stiffness degradation mechanism led to a significant overestimation of structural stiffness and an underestimation of deflections by approximately 77%. These results confirm that purely plastic models have limited applicability to cracked concrete, especially when local fracture processes and post-cracking stiffness degradation are of interest.

The comparison with full-field DIC measurements confirmed the high value of this technique as a validation tool. In contrast to traditional LVDT sensors, DIC provides strain maps that enable direct assessment of local failure mechanisms. In the present work, the comparison of crack patterns became an important criterion for evaluating the quality of the constitutive models and identified the Massicotte formulation as the closest to the experimental response.

At the same time, the combination of full-field DIC measurements and CDP simulations is associated with higher experimental and computational costs. On the experimental side, it requires careful surface preparation, optical calibration, image acquisition, and post-processing of large datasets. On the numerical side, reliable comparison with DIC maps requires refined finite element models, nonlinear damage-based analyses, convergence control, and extraction of results from the observed surface. Therefore, such validation procedures are particularly useful for research-oriented model assessment and calibration, while routine engineering design usually remains based on simpler global response indicators.

CONCLUSIONS

Based on the numerical analyses and their multi-criteria validation using DIC, the following conclusions were formulated:

1. The description of concrete behaviour in tension is decisive for the global and local response of reinforced concrete beams, governing both the load-deflection relationship and the character of crack development.
2. The highest agreement with the experimental data was achieved using the CDP model with the strain-dependent Massicotte softening function (N4). This model reproduced the nonlinear stiffness with a deflection difference of approximately -16% relative to the reference LVDT measurement.
3. The Massicotte model (N4) also provided the best overall agreement with the DIC strain maps in terms of crack density, localisation character, and vertical development of cracking.
4. Models based on stress-crack opening relationships (N5-N7) demonstrated higher numerical stability, but they underestimated deflections and produced more diffuse damage zones. This reduced their ability to reproduce individual crack paths.
5. The direct fracture energy model (N8), despite its sound theoretical basis, did not accurately reproduce the experimental crack distribution in this study. It produced fewer dominant cracks and a less developed damage pattern than observed in the DIC results.
6. Classical plasticity models (N2-N3) proved inadequate for the analysis of cracked reinforced concrete members. The absence of a damage mechanism resulted in a drastic underestimation of deflections of approximately -77%.
7. The Eurocode 2-based engineering model (N1) overestimated deflections by approximately +35% relative to the LVDT measurement, confirming its conservative character for serviceability limit state verification in standard design practice.
8. Full-field DIC monitoring provided insight into phenomena inaccessible to traditional point sensors. The additional semi-quantitative comparison of crack-pattern metrics strengthened the objectivity of the validation, although direct crack-width extraction and automated strain localisation indices remain subjects for future work.

Acknowledgements

The authors would like to thank Pekabex BET S.A. for the fabrication of the reinforced concrete beam as well as for the material and technical support provided during the experimental programme. Special acknowledgement is extended to the personnel of the Research and Development Department for conducting the full-scale experimental tests using advanced and precise measurement systems, including digital image correlation (DIC) techniques, which significantly contributed to the quality and comprehensiveness of the research programme.

REFERENCES

1. Almeida J.D.S.S.M., de Castro S.S., Leão H.M., Pitangueira R.L.S. Exploring the influence of heterogeneity on determination of an RVE for concrete structures. In: Proceedings of the XLV Ibero-Latin American Congress on Computational Methods in Engineering (CILAMCE); 2024 Nov 11-14; Maceió, Brazil. ABMEC; 2024. https://doi.org/10.55592/cilamce.v6i06.10251

2. Bazant Z.P., Novak D. Stochastic models for deformation and failure of quasibrittle structures: recent advances and new directions. In: Bicanic N., de Borst R., Mang H., Meschke G., editors. Computational Modelling of Concrete Structures (Proc. EURO-C Conf., St. Johann im Pongau, Austria). Lisse (The Netherlands): Balkema Publishing; 2003; 583–598.
3. EN 1992-1-1:2004. Eurocode 2: Design of concrete structures. Part 1-1: General rules and rules for buildings. Brussels: European Committee for Standardization (CEN); 2004.
4. Jukic M. Finite elements for modeling of localized failure in reinforced concrete [dissertation]. Cachan: École normale supérieure de Cachan; Ljubljana: Univerza v Ljubljani, Fakulteta za gradbeništvo in geodezijo; 2013. NNT: 2013DENS0064. Available from: https://theses.hal.science/tel-00997197v1
5. Long Y., Jiang Z., Zou K., Du J., Yang J. Numerical simulation analysis of the bending performance of T-beams strengthened with ultra-high-performance concrete based on the CDP model. Buildings. 2024; 14(5): 1284. https://doi.org/10.3390/buildings14051284
6. Drucker D.C., Prager W. Soil mechanics and plastic analysis for limit design. Q. Appl. Math. 1952; 10(2): 157–165. https://doi.org/10.1090/qam/48291
7. Jiang J., Wu Y. Identification of material parameters for Drucker-Prager plasticity model. Int. J. Solids Struct. 2012; 49(3–4): 567–577. https://doi.org/10.1016/j.ijsolstr.2011.10.002
8. Lubliner J., Oliver J., Oller S., Oñate E. A plastic-damage model for concrete. Int. J. Solids Struct. 1989; 25(3): 299–326. https://doi.org/10.1016/0020-7683(89)90050-4
9. Lee J., Fenves G.L. Plastic-damage model for cyclic loading of concrete. J. Eng. Mech. 1998; 124(8): 892–900. https://doi.org/10.1061/(ASCE)0733-9399(1998)124:8(892)
10. Hillerborg A., Modéer M., Petersson P.E. Analysis of crack formation and crack growth in concrete by means of fracture mechanics and finite elements. Cem. Concr. Res. 1976; 6(6): 773–781. https://doi.org/10.1016/0008-8846(76)90007-7
11. Nayal R., Rasheed H.A. Tension stiffening model for concrete beams reinforced with steel and FRP bars. J. Mater. Civ. Eng. 2006; 18(6): 831–841. https://doi.org/10.1061/(ASCE)0899-1561(2006)18:6(831)
12. Al-Manaseer A., Phillips D. Numerical study of some post-cracking material parameters affecting nonlinear solutions in RC deep beams. Can. J. Civ. Eng. 1987; 14(5): 655–666. https://doi.org/10.1139/l87-096
13. Genikomsou A.S., Polak M.A. Finite element analysis of punching shear of concrete slabs using damaged plasticity model in ABAQUS. Eng. Struct. 2015; 98: 38–48. https://doi.org/10.1016/j.engstruct.2015.04.016.
14. Szczecina M., Tworzewski P., Uzarska I. Numerical modeling of reinforced concrete beams, including the real position of reinforcing bars. Struct. Environ. 2018; 10(1): 28–38. https://doi.org/10.30540/sae-2018-003
15. Sun W., Weldon B., McGinnis M., Jiang R. Numerical and digital image correlation study of the flexural behavior of prestressed ultra-high-performance concrete beams made from locally available materials. PCI J. 2024; 69(1): 22–39. https://doi.org/10.15554/pcij69.1-01
16. Sjölander A., Belloni V., Peterson V., Ledin J. Experimental dataset to assess the structural performance of cracked reinforced concrete using digital image correlation techniques with fixed and moving cameras. Data Brief. 2023; 51: 109703. https://doi.org/10.1016/j.dib.2023.109703
17. Zhang Y., Chow C.L., Lau D. Artificial intelligence-enhanced non-destructive defect detection for civil infrastructure. Autom. Constr. 2025; 171: 105996. https://doi.org/10.1016/j.autcon.2025.105996
18. Krishna B., Reddy G., Tadepalli T., Pancharathi R., Yerra L. Numerical and experimental study on flexural behavior of reinforced concrete beams: digital image correlation approach. Comput. Concr. 2019; 24(6): 561–573. https://doi.org/10.12989/cac.2019.24.6.561.
19. Leppänen J., Johansson M., Grassl P. On the dynamic response of reinforced concrete beams subjected to drop weight impact. Finite Elem. Anal. Des. 2020; 180: 103438. https://doi.org/10.1016/j.finel.2020.103438
20. Marzec I., Bobiński J. Performance of isotropic constitutive laws in simulating failure mechanisms in scaled RC beams. Arch. Mech. 2020; 72(3): 193–215. https://doi.org/10.24423/aom.3443.
21. Al-Ateyat A., Barakat S., Junaid M.T., Altoubat S., Maalej M., Awad R. Experimental and Numerical Analysis of Punching Shear of GFRP-RC Slabs. Civil Engineering Journal. 2025; 10: 344–358. https://doi.org/10.28991/CEJ-SP2024-010-017
22. Chu T.S.C., Sorilla J., Chua A.Y. UAV-based structural health monitoring using a two-stage CNN model with lighthouse localization in GNSS-denied environments. HighTech and Innovation Journal. 2025; 6(2): 398–410. https://doi.org/10.28991/HIJ-2025-06-02-03
23. Dejene H., Bogale M., Rynkovskaya M. Numerical analysis of the shear behavior of shallow-wide concrete beams via the concrete damage plasticity model. Civil Engineering Journal. 2025; 11(2). https://doi.org/10.28991/CEJ-2025-011-02-022
24. Ribeiro P.O., Gidrão G.M.S., Vareda L.V., Carrazedo R., Malite M. Numerical and experimental study of concrete I-beam subjected to bending test with

cyclic load. Lat. Am. J. Solids Struct. 2020; 17(3): e25880. https://doi.org/10.1590/1679-78255880
25. Seemab F., Schmidt M., Baktheer A., Classen M., Chudoba R. Automated detection of propagating cracks in RC beams without shear reinforcement based on DIC-controlled modeling of damage localization. Eng. Struct. 2023; 286: 116118. https://doi.org/10.1016/j.engstruct.2023.116118
26. Çankaya M.A., Akan Ç. An experimental and numerical investigation on the bending behavior of fiber reinforced concrete beams. Turk. J. Civ. Eng. 2023; 34(1): 59–78. https://doi.org/10.18400/tjce.1209152.
27. Chandra J., Christian Y.B., Ardenlie F.G., Wibowo H. Validation of nonlinear finite element model of reinforced concrete beams subjected to monotonic loading. E3S Web Conf. 2023; 429: 05019. https://doi.org/10.1051/e3sconf/202342905019
28. Rakic D., Bodić A., Milivojevic N., Dunić V., Živković M. Concrete damage plasticity material model parameters identification. J. Serb. Soc. Comput. Mech. 2021; 15(2): 111–122. https://doi.org/10.24874/jsscm.2021.15.02.11
29. Kedziora S., Anwaar O. Concrete-filled steel tubular (CFTS) columns subjected to eccentric compressive load. AIP Conf. Proc. 2019; 2060: 020004. https://doi.org/10.1063/1.5086135
30. Szwed A., Kamińska I. A general form of Drucker-Prager type smooth and convex plastic potential. Part 1: Definition and features. MATEC Web Conf. 2018; 196: 01040. https://doi.org/10.1051/matecconf/201819601040
31. Neuberger Y.M., Andrade M.V., de Sousa A.M.D., Bandieira M., da Silva Júnior E.P., dos Santos H.F., Catoia B., Bolandim E.A., de Moura Aquino V.B., Christoforo A.L., Ferreira M.A. Numerical analysis of reinforced concrete corbels using concrete damage plasticity: sensitivity to material parameters and comparison with analytical models. Buildings. 2023; 13(11): 2781. https://doi.org/10.3390/buildings13112781
32. Rong Y., Ren H., Xu X. An improved damage-plasticity material model for concrete subjected to dynamic loading. Case Stud. Constr. Mater. 2023; 19: e02568. https://doi.org/10.1016/j.cscm.2023.e02568.
33. Sargin M. Stress-strain relationship for concrete and the analysis of structural concrete section. SM Studies Series, Study No. 4. Waterloo (ON): University of Waterloo, Solid Mechanics Division; 1971.
34. Jankowiak T., Łodygowski T. Identification of parameters of concrete damage plasticity constitutive model. Found. Civ. Environ. Eng. 2005; (6): 53–69.
35. Kasilingam S., Sharma R. Estimation on accuracy of compressive and tensile damage parameters of concrete damage plasticity model. In: Dimitrovová Z., Biswas P., Gonçalves R., Silva T., editors. Recent Trends in Wave Mechanics and Vibrations. Mechanisms and Machine Science, vol. 125. Cham: Springer; 2023. https://doi.org/10.1007/978-3-031-15758-5_6
36. Massicotte B., Elwi A.E., MacGregor J.G. Tension-stiffening model for planar reinforced concrete members. J. Struct. Eng. 1990; 116(11): 3039–3058. https://doi.org/10.1061/(ASCE)0733-9445(1990)116:11(3039)
37. Allam S.M., Shoukry M.S., Rashad G.E., Hassan A.S. Evaluation of tension stiffening effect on the crack width calculation of flexural RC members. Alex. Eng. J. 2013; 52(2): 163–173. https://doi.org/10.1016/j.aej.2012.12.005.
38. Hafezolghorani Esfahani M., Hejazi F., Vaghei R., Jaafar M.S.B., Karimzadeh K. Simplified damage plasticity model for concrete. Struct. Eng. Int. 2017; 27(1): 68-78. https://doi.org/10.2749/101686616X1081
39. Croce P., Formichi P. Numerical simulation of the behavior of cracked reinforced concrete members. Mater. Sci. Appl. 2014; 5(12): 883–892. https://doi.org/10.4236/msa.2014.512090
40. Roelfstra P.E., Wittmann F.H. Numerical method to link strain softening with failure of concrete. In: Wittmann F.H., editor. Fracture Toughness and Fracture Energy of Concrete. Developments in Civil Engineering, vol. 18. Amsterdam: Elsevier; 1986.
41. Fédération Internationale du Béton (fib). fib Model Code for Concrete Structures 2010. Berlin: Ernst & Sohn; 2013.
42. Hillerborg A. The theoretical basis of a method to determine the fracture energy GF of concrete. Mater. Struct. 1985; 18(4): 291–296. https://doi.org/10.1007/BF02472919
43. Cornelissen H.A.W., Hordijk D., Reinhardt H.W. Experimental determination of crack softening characteristics of normalweight and lightweight concrete. Heron. 1986; 31(2).
44. Guo L., Xiang J., Latham J.P., Izzuddin B.A. A numerical investigation of mesh sensitivity for a new three-dimensional fracture model within the combined finite-discrete element method. Eng. Fract. Mech. 2015; 151. https://doi.org/10.1016/j.engfracmech.2015.11.006
45. Abdolpour H., Sawicki B. Analyzing fracture mechanism of high performance concrete using concrete damage plasticity model. Arch. Civ. Mech. Eng. 2025; 25(5–6). https://doi.org/10.1007/s43452-025-01287-3
46. Dassault Systèmes. Abaqus [software]. Version 2025. Providence (RI): Dassault Systèmes; 2025. Abaqus User Subroutines Reference Guide: Concrete Damage Plasticity. Available-from: http://130.149.89.49:2080/v2016/books/usb/default.htm?startat=pt05ch23s06abm39.html